

## Optical detection of folded mini-zone-edge coherent acoustic modes in a doped GaAs/AlAs superlattice

R. Beardsley,<sup>1</sup> A. V. Akimov,<sup>1</sup> B. A. Glavin,<sup>2</sup> W. Maryam,<sup>1</sup> M. Henini,<sup>1</sup> and A. J. Kent<sup>1</sup>

<sup>1</sup>*School of Physics and Astronomy, University of Nottingham, University Park, Nottingham NG7 2RD, United Kingdom*

<sup>2</sup>*V. E. Lashkarev Institute of Semiconductor Physics, Pr. Nauki 41, Kiev 03028, Ukraine*

(Received 2 March 2010; revised manuscript received 16 June 2010; published 15 July 2010)

A coherent phonon mode with frequency corresponding to the first mini Brillouin-zone edge stop gap is observed in ultrafast pump-probe measurements on a doped semiconductor superlattice structure. It is proposed that the optical detection of the mode is facilitated by interactions with the free carriers present in the superlattice.

DOI: [10.1103/PhysRevB.82.041302](https://doi.org/10.1103/PhysRevB.82.041302)

PACS number(s): 73.21.Cd, 63.20.kd, 63.22.Np, 72.80.Ey

Owing to variations in the acoustic impedance on a period  $d_{\text{SL}}$  in a superlattice (SL) structure, the acoustic-phonon dispersion is “folded” into a mini-Brillouin zone. Stop gaps open up in the dispersion at the mini-zone-center (phonon wave vector  $q=0$ ) and mini-zone edge ( $q=\pi/d_{\text{SL}}$ ) due to Bragg reflection of phonons in the structure. The folded phonons have been extensively studied using Raman scattering<sup>1,2</sup> and ultrafast optical pump-probe measurement.<sup>3–9</sup> The latter technique is able to measure the coherent nature of the phonon modes excited in the structure and their decay time. Experimentally observed elastic modes normally follow the momentum conservation selection rules in the photon-phonon interactions. In backscattering and forward-scattering geometry, these Raman-active modes correspond to phonon wave vectors  $q \leq 2k$  ( $k$ -photon wave vector in SL). For SLs having typical dimensions with  $d_{\text{SL}} \sim 10$  nm and probing by visible light, this means modes with wave vectors close to the center of the Brillouin mini zone. Hereinafter we will refer to these as the *c* modes. Modes near the mini-zone edge with  $q > 2k$  are not normally expected to be detected in optical measurements on a SL due to the inability to conserve momentum in the phonon-photon interactions.

In practice, the momentum conservation may be partially relaxed due to the finite size of SLs compared with the optical wavelength, fluctuations in the thickness of the SL layers, and the limited penetration depth of light into SL.<sup>10</sup> This opens the possibility of operating optically with modes falling close to the mini-zone-edge stop gaps. Incoherent detection of these modes, which we will call the *e* modes, has been observed in stationary Raman experiments.<sup>10,11</sup> However, to our knowledge, there have been no reports of the detection of coherent *e* modes in ultrafast pump-probe measurements on SLs, except in specially designed samples incorporating phonon nanocavities,<sup>12</sup> where SLs each side of the cavity act as Bragg mirrors for the *e* mode.

Here we report excitation and detection of the *e* mode ( $q \approx \pi/d_{\text{SL}}$ ) in a single SL structure without a nanocavity using ultrafast pump-probe experiments. For certain photon probing energies and temporal delays, this mode becomes dominant in the detected coherent vibrational spectrum. In view of the absence of the *e* mode in the numerous similar measurements on SLs reported in the literature, this result is very surprising. However, what sets our sample apart from

the many different SLs previously studied, which possessed a wide range of different layer thickness parameters, is the presence of free carriers in the SL due to intentional silicon doping of the layers. We propose that it is the presence of these free carriers providing also a momentum relaxation path which allows selective optical generation and detection

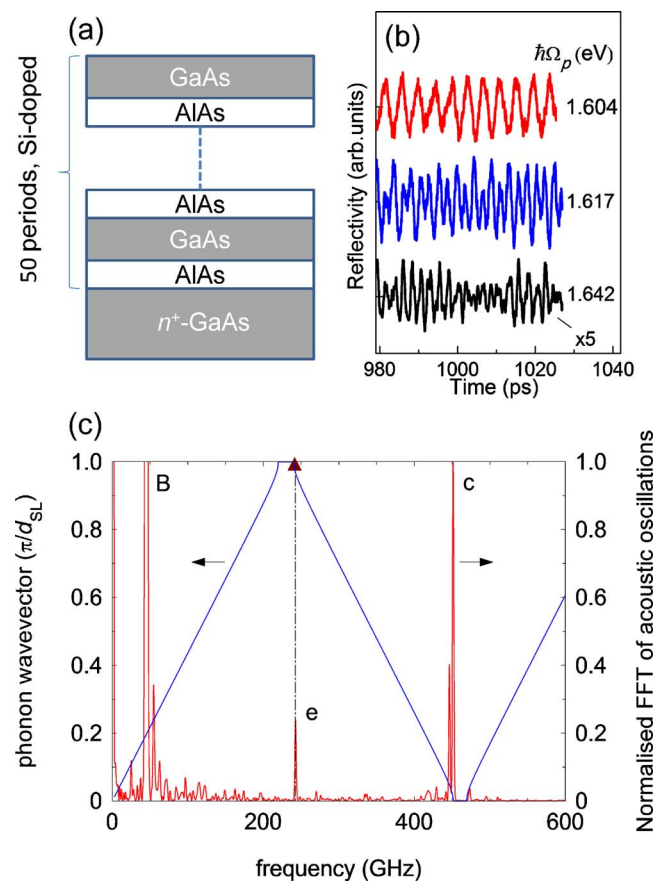


FIG. 1. (Color online) (a) The structure of the studied SL. (b) Fragments of the temporal traces of the pump-probe reflectivity  $\Delta R(t)$  measured at three photon energies  $\hbar\Omega_p$ . (c) The Fourier power spectrum  $P_f$  (normalized to the *c* mode) for  $\hbar\Omega_p = 1.604$  eV; the peaks corresponding to the Brillouin backscattering mode and the edge and center SL modes are labeled as “B,” “e,” and “c,” respectively. Also shown in (c) is the folded longitudinal phonon dispersion calculated for the SL.

of the e mode in our experiments. The observation of the e mode in a straightforward single-SL structure could suggest the feasibility of efficient terahertz (THz) phonon confinement structures even without phonon nanocavities, which is important for development of corresponding phononic and optophononic applications.

The experimental structure, Fig. 1(a), was grown on  $n^+$ -(001) GaAs by molecular-beam epitaxy. It consisted of a 50-period SL ( $d_{\text{SL}} \approx 9.8$  nm), each period made up from nominal thicknesses 5.9 nm of GaAs and 3.9 nm of AlAs, and with a GaAs layer at the top. The SL was uniformly  $n$  doped with Si to a density of  $\sim 10^{16}$  cm $^{-3}$ . On the basis of these SL parameters, we estimate that the sheet electron density per GaAs quantum well (QW) is about  $10^{10}$  cm $^{-2}$ . This gives a Fermi energy of about 0.3 meV, and, using the Kronig-Penney model, we determine the electron miniband width to be about 1 meV. Measurements were made with the sample at a temperature of 11 K. The standard reflection pump-probe technique for studying coherent phonons in SLs was employed: 150 fs pulses with a repetition rate of 82 MHz were provided by a tunable ( $\lambda = 690\text{--}1050$  nm) mode-locked Ti:Sapphire laser. The pump beam was chopped at a frequency of 50 KHz using an acousto-optic modulator and then focused to a spot of diameter 100  $\mu\text{m}$  on the sample surface. The probe beam was focused on the sample to a spot of diameter less than 50  $\mu\text{m}$  within the pump spot. The energy densities in the pulses of the pump and probe beams were  $\sim 10$   $\mu\text{J}/\text{cm}^2$  and  $\sim 1$   $\mu\text{J}/\text{cm}^2$ , respectively. The time delay between the pump pulse and probe pulse was provided by three optical delay lines. In the pump path there was retroreflector mounted on a shaker providing fast, 2.5 Hz, scanning of up to 55 ps window centered on a time  $t_0$ , also in the pump path was a step-motor delay line for fine adjustment of  $t_0$  within a 1 ns window. In the probe path there was a manual delay stage enabling coarse adjustment of  $t_0$  up to 3 ns. The reflection  $R(t)$  of the probe from the sample surface was detected as a function of the shaker delay  $t$  by a photodiode and lock-in amplifier referenced to the pump modulation. The output of the lock-in amplifier was fed to an averaging oscilloscope which was synchronized with the shaker delay line.

Figure 1(b) shows the reflectance changes  $\Delta R(t) = R(t) - R_0$  ( $R_0$  is the reflectivity without pump excitation) as a function of the delay time  $t$  between the pump and probe pulses in 50 ps fragments centered on  $t_0 = 1$  ns and measured for three different photon energies  $\hbar\Omega_p$  emitted from the laser. Figure 1(c) shows the spectral density  $P_f$  at  $\hbar\Omega_p = 1.604$  eV, which was obtained by taking the fast Fourier transform of  $\Delta R(t)$  over the pump-probe delay range 0–670 ps. The elastic modes which contribute to  $\Delta R(t)$  are in three frequency ranges: the Brillouin backscattering mode at about 45 GHz; the high-frequency Brillouin mini-zone-center modes (c modes) at about 450 GHz; and the low-frequency mini-zone-edge modes (e modes) at about 240 GHz. It is clearly seen that the time evolution of  $\Delta R(t)$  and the corresponding  $P_f$ , which are shown in Fig. 2, strongly depend on  $\hbar\Omega_p$ . For example, in the 50 ps window at  $t_0 = 1$  ns, the e mode is dominant at  $\hbar\Omega_p = 1.604$  eV [upper curves in Figs. 1(b) and 2]. At  $\hbar\Omega_p = 1.642$  eV the high-frequency c mode with has the highest amplitude

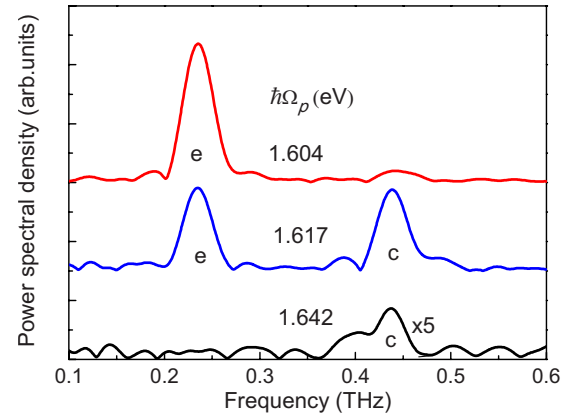


FIG. 2. (Color online) The Fourier spectra  $P_f$  obtained from the corresponding temporal traces shown in Fig. 1(b).

[lower curves in Figs. 1(b) and 2]. In the general case, both e and c modes are detected in a range of  $\hbar\Omega_p$  close to the fundamental exciton resonance of the GaAs QWs forming the SL, which was determined by photoreflectance and photoconductance measurements to be 1.6 eV ( $\pm 10$  meV).

The high-frequency c modes with  $q \approx 0$  have been observed earlier in a number of previous experiments,<sup>4–6,9,13</sup> and the presence of this mode in the measured  $\Delta R(t)$  is not surprising. In agreement with earlier studies,<sup>4,5,13</sup> in the present low-temperature experiment, the amplitude of the coherent vibrations is sensitive to  $\hbar\Omega_p$ . However, the experimental fact that at some  $\hbar\Omega_p$ , the low-frequency e mode becomes dominant in  $\Delta R(t)$  is contrary to the traditional photoelastic approach.

The main task of the following discussion is to present a qualitative explanation for the origin of the low-frequency e mode ( $q \approx \pi/d_{\text{SL}}$ ) in the measured signals. We consider the microscopic mechanism of detection and generation of coherent elastic vibrations in SL: at low temperature this is commonly believed to be due to the resonant coupling of two-dimensional excitons in the GaAs QWs forming the SL with the pump and probe electromagnetic wave. Since the strain associated with the lattice vibrations shifts the exciton energy levels due to deformation-potential mechanism, the dielectric properties of the SL QW layers are modulated. At first sight, it is not expected that modes with  $q \approx \pi/d_{\text{SL}}$  will provide a contribution to the light modulation. Indeed, for such modes, the elastic strain in adjacent QWs of the SL oscillates in antiphase which is expected to suppress modulation of the probe light in the detection process. However, as we shall argue below, the Coulomb coupling of free carriers present in the doped SL with the excitons, could result in modulation of the probe light by the e mode. Additionally, interaction with the free carriers also enables momentum to be conserved. Such interactions are well known for the case of slightly doped single QWs,<sup>14</sup> here we assume that it is reasonable to consider such interactions in the multiple QWs forming the SL. Indeed, the likely importance of the free carriers due to doping is confirmed by measurements in the same experimental setup on a similar, but undoped, GaAs/AlAs SL, in which we could not detect the e mode at any  $\hbar\Omega_p$ .

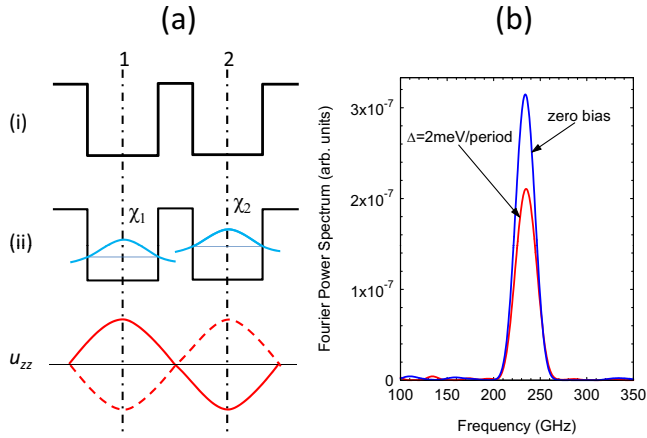


FIG. 3. (Color online) (a) Schematic showing a pair of neighboring QWs (1 and 2) in the SL and the acoustic  $e$  mode  $u_{zz}$  of importance for coupling with the electrons in the SL. In the case (i) an electron miniband is formed but in the case (ii) the band is destroyed by disorder. (b) The effect on the amplitude of the  $e$  mode of applying an electrical bias to increase the energy shift,  $\Delta$ , between the wells.

In a SL where an electron miniband is formed, the momentum and energy conservation conditions are satisfied if the  $\pi/d_{SL}$  momentum of the  $e$  mode is transferred to the electron momentum perpendicular to the SL plane. In our case, the tunneling coupling in the SL is weak and the narrow electron miniband is likely to be destroyed by disorder. However, it can be shown that, even in the case of two-well tunneling coupling, the necessary momentum can be accommodated by coupling to the states involving electrons in neighboring QWs. In fact, we have to consider the three-particle state composed from electron and hole confined in one QW and an electron confined in the nearest-neighbor QW coupled to each other by the Coulomb interaction [see Fig. 3(a)]. For weak tunnel coupling, the wave functions of electrons confined in the first and second QWs can be written:  $\psi_1 = \chi_1 + \frac{T}{\Delta}\chi_2$ ;  $\psi_2 = \chi_2 - \frac{T}{\Delta}\chi_1$ , where  $\chi_{1,2}$  are the wave functions corresponding to electrons confined in decoupled QWs,  $T$  is the tunneling matrix element, and  $\Delta$  is shift of the levels in the QWs caused by disorder. The latter is estimated to be on the order 1 meV in our SL. These expressions, which are strictly valid for the case  $\frac{T}{\Delta} \ll 1$ , reflect the dependence on only the  $z$  coordinate, which is perpendicular to the SL layers, and it must be complemented by the proper lateral dependence, which is controlled by the Coulomb interaction. The latter, however, is not important for the strain-induced energy shift of the related many-electron state. Within the deformation-potential approach, the electron portion of such shift is determined as

$$\delta E = \Xi \frac{T}{\Delta} \left( \int u_{zz} \chi_2^2 dz - \int u_{zz} \chi_1^2 dz \right), \quad (1)$$

where  $u_{zz}$  is the phonon-induced strain and  $\Xi$  is electron deformation-potential constant, and  $q_s$  is the phonon wave vector. As can be seen, because  $u_{zz}$  for  $e$  modes has opposite sign in adjacent QWs, the contributions of the different pairs

of QWs are added to each other thus enable modulation of the probe by the  $e$  mode. Furthermore, the electron confined in the QW is able to “absorb” the excess momentum provided this is less than  $q_{\max} \sim \pi/w$ , where  $w$  is the well width.<sup>15</sup> In this case  $w = 5.9$  nm, which means  $q_{\max} = 5.3 \times 10^8 \text{ m}^{-1}$ , which is indeed greater than the momentum of the  $e$  mode ( $\pi/d_{SL} = 3.2 \times 10^8 \text{ m}^{-1}$ ).

It is apparent from Eq. (1) that increasing  $\Delta$  should result in a decrease in the coupling between neighboring wells and hence suppression of the optical detection of the  $e$  mode. One way of increasing  $\Delta$  in order to test this prediction is to apply an electrical bias to the SL. To do this we fabricated a device with electrical contacts at each end of the SL. With zero electrical bias applied, the  $c$  and  $e$  modes were detected in similar ratio as in the sample with no contacts, thus showing that the presence of the electrical contact layers does not change significantly the acoustic modes of the system. The effect on the  $e$  mode of applying a dc bias is shown in Fig. 2(b). Here the Fourier power spectrum was obtained in a 50 ps wide window centered at a pump-probe delay of 2 ns. As expected, application of the dc bias leads to suppression of the  $e$  mode. We should point out that, at the maximum applied electric field of  $2000 \text{ V cm}^{-1}$ , the Stark effect in the QWs has a negligible ( $\ll 1$  meV) effect on the energies of the optical transitions as confirmed by the photoconductance measurements, and consistent with reports in Ref. 16.

Of course, the above model provides only a very qualitative explanation for the detection of  $e$  modes. Rigorously, the spectrum of such three-particle excitations, their coupling to electromagnetic radiation, and statistics of the level shift distribution must be addressed in order to account for the detailed dependence on  $\hbar\Omega_p$ . This will be the subject of future work, but one might reasonably expect the interactions to result in the optimum photon energy for detection of the  $e$  modes to be slightly shifted compared to that for detection of the  $c$  modes, as is observed in the experiments.

The overall relative contribution of various elastic modes to the detected  $\Delta R(t)$  and hence  $P_f$  at a certain delay  $t_0$  is governed by their detection, generation and decay. The generation of coherent THz vibrations is attributed to a number of physical mechanisms, including the photoelastic effect and deformation potential.<sup>17,18</sup> Depending on the pump photon energy,  $\hbar\Omega_p$ , the first or the second of these may play a dominant role in generation of Raman  $c$  modes. The generation of the specific  $e$  mode may be considered in a similar way to the detection process described above. In any case, the amplitude of the  $e$ -mode signal initially generated by an optical pump pulse at  $t=0$  is not expected to be larger than that for Raman-active modes. This statement is consistent with the experimental results obtained at the early times when  $c$  mode is always dominant in the measured vibrational spectrum, Fig. 4.

In the experiments, the  $e$  mode becomes totally dominant only at long-time delays, which suggests that its lifetime  $\tau_e$  is significantly longer than the lifetime  $\tau_c$  of  $c$  modes. Figure 4(a) shows  $P_f$  for various time delays  $t_0$ . At early times ( $t_0 < 300$  ps) high-frequency  $c$  modes in the range 400–550 GHz are dominant in the spectrum, in agreement with earlier observations.<sup>4–9</sup> The backscattering Raman mode with  $q=2k$  is expected to escape from the SL in time

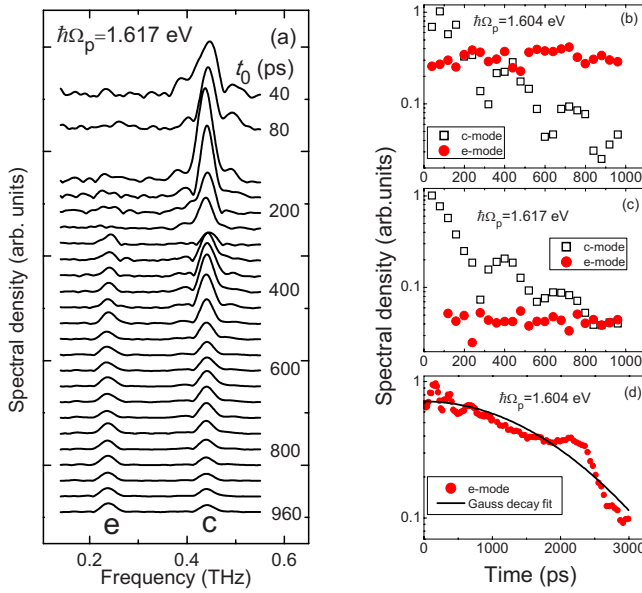


FIG. 4. (Color online) (a) Spectral density  $P_f$  measured for various delays  $t_0$ . [(b)–(d)] Time evolutions of the spectral density integrated over 60 GHz range for c (open squares) and e (solid circles) modes. The temporal window for obtaining fast Fourier transform was [(a)–(c)] 50 ps and (d) 18 ps.

$\tau_R \sim 2l/s_{LA} \sim 200$  ps, where  $l=490$  nm is the thickness of SL and  $s_{LA} \approx 5 \times 10^3$   $\text{ms}^{-1}$  is a longitudinal sound velocity in the SL. Thus, when the delay  $t_0 \gg \tau_R$  the spectrum,  $P_f$ , should consist only of modes which have low group velocity ( $q \approx 0$  or  $q \approx \pi/d_{SL}$ ). Figure 4(a) shows that in the experiments these modes remain as two clearly distinguished spectral lines in  $P_f$  only at delays  $t_0 > 300$  ps. The time evolutions of the  $P_f$  integrated over the range of 60 GHz for c and

e modes are shown in Figs. 4(b)–4(d). The decay of the c modes is known to have nontrivial evolution, which includes beatings between various c modes [see open symbols in Figs. 4(b) and 4(c)]. This causes complications in obtaining precisely their lifetime. However from the results presented in Fig. 4 it is obvious that the c modes decay at a rate much faster than the e mode.

A large part of the difference in lifetimes for c and e modes can be explained if their decay is due to lateral fluctuations of the SL layer thickness giving rise to the dephasing of the coherent oscillations.<sup>19</sup> Assuming a Gaussian distribution of such fluctuations, we predict the decay of the measured signal,  $\sim \exp[-t^2/(2\tau^2)]$  and due to difference in frequencies we would get  $\tau_c \approx \tau_e/2$ , where  $\tau_c$  and  $\tau_e$  correspond, respectively, to the c and e modes. Fitting the experimentally measured decay for the e mode in the interval up to 3 ns by a Gaussian decay curve, shown by solid line in Fig. 4(d), we get  $\tau_e \approx 1.6$  ns. For the c modes the observed decay is more than twice as fast and closer to exponential in shape, which implies there may also be contributions to the c mode decay from other mechanisms, e.g., phonon-scattering processes and anharmonicity, which increase in strength with increasing frequency.

In conclusion, using the ultrafast optical pump-probe technique, we detect the coherent elastic oscillations with frequency corresponding to the edge of the first folded acoustic mini-Brillouin zone in a doped GaAs/AlAs SL. We have proposed a qualitative explanation of this observation in terms of interactions with the free electrons, which permits coupling of the e modes with photons having  $k$  near the Brillouin-zone center.

We acknowledge EPSRC and Royal Society for financial support of this work.

- <sup>1</sup>C. Colvard, R. Merlin, M. V. Klein, and A. C. Gossard, *Phys. Rev. Lett.* **45**, 298 (1980).
- <sup>2</sup>B. Jusserand and M. Cardona, in *Light Scattering in Solids V*, Topics in Applied Physics, edited by M. Cardona and G. Güntherodt (Springer, Heidelberg, 1989), Vol. 66, p. 49.
- <sup>3</sup>W. Chen, Y. Lu, H. J. Maris, and G. Xiao, *Phys. Rev. B* **50**, 14506 (1994).
- <sup>4</sup>A. Yamamoto, T. Mishina, Y. Masumoto, and M. Nakayama, *Phys. Rev. Lett.* **73**, 740 (1994).
- <sup>5</sup>A. Bartels, T. Dekorsy, H. Kurz, and K. Köhler, *Phys. Rev. Lett.* **82**, 1044 (1999).
- <sup>6</sup>K. Mizoguchi, M. Hase, S. Nakashima, and M. Nakayama, *Phys. Rev. B* **60**, 8262 (1999).
- <sup>7</sup>C.-K. Sun, J.-C. Liang, and X.-Y. Yu, *Phys. Rev. Lett.* **84**, 179 (2000).
- <sup>8</sup>E. Makarona, B. Daly, J.-S. Im, H. Maris, A. Nurmikko, and J. Han, *Appl. Phys. Lett.* **81**, 2791 (2002).
- <sup>9</sup>M. Trigo, T. A. Eckhause, M. Reason, R. S. Goldman, and R. Merlin, *Phys. Rev. Lett.* **97**, 124301 (2006).
- <sup>10</sup>T. Ruf, V. I. Belitsky, J. Spitzer, V. F. Sapega, M. Cardona, and K. Ploog, *Phys. Rev. Lett.* **71**, 3035 (1993).

- <sup>11</sup>V. F. Sapega, V. I. Belitsky, T. Ruf, H. D. Fuchs, M. Cardona, and K. Ploog, *Phys. Rev. B* **46**, 16005 (1992).
- <sup>12</sup>M. F. Pascual Winter, G. Rozas, A. Fainstein, B. Jusserand, B. Perrin, A. Huynh, P. O. Vaccaro, and S. Saravanan, *Phys. Rev. Lett.* **98**, 265501 (2007).
- <sup>13</sup>F. Hudert, A. Bartels, C. Janke, T. Dekorsy, and K. Köhler, *J. Phys.: Conf. Ser.* **92**, 012012 (2007).
- <sup>14</sup>G. Finkelstein, H. Shtrikman, and I. Bar-Joseph, *Phys. Rev. Lett.* **74**, 976 (1995).
- <sup>15</sup>*Electron-Phonon Interactions in Low-Dimensional Structures*, edited by L. J. Challis (Oxford Science, Oxford, 2003).
- <sup>16</sup>*Semiconductor Superlattices: Growth and Electronic Properties*, edited by H. T. Grahn (World Scientific, Singapore, 1995).
- <sup>17</sup>G. D. Sanders, C. J. Stanton, and C. S. Kim, *Phys. Rev. B* **64**, 235316 (2001).
- <sup>18</sup>P. Walker, R. P. Champion, A. J. Kent, D. Lehmann, and Cz. Jasiukiewicz, *Phys. Rev. B* **78**, 233307 (2008).
- <sup>19</sup>G. Rozas, M. F. Pascual Winter, B. Jusserand, A. Fainstein, B. Perrin, E. Semenova, and A. Lemaître, *Phys. Rev. Lett.* **102**, 015502 (2009).